43rd AIAA Aerospace Sciences Meeting and Exhibit
10-13 January, 2005, Reno, Nevada

AIAA 2005-0320

Multi-Dimensional Spectral Difference Method for Unstructured Grids

Yen Liu*
NASA Ames Research Center, Moffett Field, CA 94035

Marcel Vinokur†
Eloret Corp, Sunnyvale, CA 94086

and

Z. J. Wang‡
Iowa State University, Ames, IA 50011

A new, high-order, conservative, and efficient method for conservation laws on unstructured grids is developed. It combines the best features of structured and unstructured grid methods to attain computational efficiency and geometric flexibility; it utilizes the concept of discontinuous and high-order local representations to achieve conservation and high accuracy; and it is based on the finite-difference formulation for simplicity. Universal reconstructions are obtained by distributing unknown and flux points in a geometrically similar manner for all unstructured cells. Placements of these points with various orders of accuracy are given for triangular and tetrahedral elements. Accuracy studies of the method are carried out with the two-dimensional linear wave equation and Burgers' equation, and each order of accuracy is numerically verified. Numerical solutions of plane electromagnetic waves incident on perfectly conducting circular cylinders and spheres are presented and compared with the exact solutions to demonstrate the capability of the method. Excellent agreements have been found. The method is simpler and more efficient than previous discontinuous Galerkin and spectral volume methods for unstructured grids.

Nomenclature

d	=	dimension of the domain
F	=	generalized flux
i	=	index for cell
j	=	index for unknown u
k	=	index for flux F
l	=	index for face
L_j	=	cardinal basis or shape function for unknown u
M_k	=	cardinal basis or shape function for flux F
$\mathbf{r}_j$	=	unknown location
$\mathbf{r}_k$	=	flux location
$\mathbf{S}$	=	face area
V	=	cell volume
u	=	conservative variable

* Research Scientist, Yen.Liu@nasa.gov, Mail Stop T27B-1, AIAA Member.
† Research Scientist, vinokur@nas.nasa.gov, AIAA Associate Fellow.
‡ Associate Professor, Department of Aerospacel Engineering, zjw@iastate.edu, AIAA Associate Fellow.

I. Introduction

A current problem of great interest is to obtain very high-order accurate and efficient numerical solutions of systems of conservation laws for complex shapes. There are two types of computational grids, namely structured and unstructured grids. For most problems with complex shapes, unstructured grids consisting of triangles in 2D and tetrahedra in 3D are preferred because of the relatively short grid generation time. The most commonly used unstructured method is the finite-volume (FV) method, applied to the integral form of the conservation law with cell averages of the conservative variables as the unknowns [1,6,10]. A reconstruction of any desired order of accuracy for each cell is obtained in terms of unknowns at neighboring cells. The flux integral for each face is evaluated using the reconstructed solution for the two cells and an approximate Riemann solver. For non-linear flux functions, a quadrature approximation is employed. Thus, conservation is satisfied locally for each cell. However, due to the unstructured nature of the grid, it is difficult to obtain a non-singular stencil. This necessitates a least-squares inversion in general. For very high order of accuracy, the number of cells in the stencil, and thus the number of operations to carry out the numerical procedure, can become very large in three dimensions. This would hamper the efficiency of the method. Furthermore, since each unknown employs a different stencil, one must repeat the least-squares inversion for every cell at each time step, or to store the inversion coefficients. In a high-order, three-dimensional computation, the former would involve impractically large CPU times, while for the latter the memory requirement becomes prohibitive. In addition, the data from neighboring cells required for the computation can be far apart in memory. This further hampers the efficiency of the method due to data gathering and scattering. As a result of these deficiencies, the FV method is limited to second order accuracy in most applications.

Finite element (FE) methods [7] have long been used for unstructured grids because of their geometric flexibility. A major difference between the FE and the FV methods is that the former seeks reconstruction data from within the cell (or element), while the latter employs the data from outside the cell. In the FE formulation, unknowns are nodal values, which are placed at geometrically similar points in each element. Due to this geometric similarity, the local reconstruction becomes universal for all cells in terms of the same set of cardinal basis or shape functions. By assigning a single value to the nodes on cell boundaries, a global piecewise continuous reconstruction can be obtained. The conservative equations are then satisfied in a weak form by multiplying them with the requisite number of test functions, integrating over the global domain, and using integration by parts. This results in a set of coupled equations for all the unknowns. Their solution involves a very large, sparse matrix, whose elements depend on the cell geometries. For nonlinear equations, quadrature approximations are necessary to evaluate the matrix elements. While the integral conservation law is satisfied for the global domain, it is not satisfied locally for each cell.

To overcome the deficiencies of the FE method for conservation laws, the discontinuous Galerkin (DG) method was developed [2-5]. Nodes on cell boundaries are allowed to have multiple values, so that the local reconstruction in each cell is in general discontinuous with that of its neighbors. The integration is carried out over each element, using the local shape functions as the test functions. As in the FV method, a Riemann solver is employed at cell boundaries. The integral conservation law is now satisfied for each cell. While we must still solve sets of coupled equations, each set now only involves the unknowns in one element. In addition, since the integrals involve quadratic terms, the quadrature formulas must have twice the degree of precision as the precision of the reconstruction.

The spectral volume (SV) method [12,18-21] overcomes the computational inefficiencies of the FV method by adopting the FE concept of using only data within the cell for reconstruction. Each triangular or tetrahedral cell, here called a spectral volume (SV), is partitioned into structured subcells called control volumes (CV). These are polygons in 2D, and polyhedra in 3D. The latter can have non-planar faces, which must be subdivided into planar facets in order to perform flux integrations. The unknowns are now cell averages over the CV's. If the SV's are partitioned in a geometrically similar manner, a single, universal reconstruction results. Thus only a few coefficients need to be stored in advance to evaluate all flux integrals. For high orders of accuracy in 3D, the partitioning requires the introduction of a large number of parameters, whose optimization to achieve convergence becomes increasingly more difficult. The growth in the number of interior facets and the increase in the number of quadrature points for each facet, raises the computational cost greatly.

An alternate method for unstructured grids is the finite-difference (FD) method [17], applied to the differential form of the conservation law with values of the conservative variables at grid nodes as the unknowns. Actually, one only needs an arbitrary set of nodal points, without the connections that define a grid. One again employs a local reconstruction in terms of neighboring unknowns, but the method is simpler than the FV method, since one only needs to differentiate the reconstructed solution. In addition to all the disadvantages of the latter, the method is not locally conservative.

In this paper, we introduce a new, high-order, conservative, and efficient method, named the spectral difference (SD) method, for conservation laws on unstructured grids. The method combines the best features of structured and unstructured grid methods to attain computational efficiency and geometric flexibility. It utilizes the concept of discontinuous and high-order local representations to achieve conservation and high accuracy in a manner similar to the DG and SV methods, but the new method is based on the finite-difference formulation to attain a simpler form and higher efficiency. In the next section, we first describe the basic formulation of the method. Some representative placements of the unknown and flux points with various orders of accuracy for triangular and tetrahedral elements are then presented in Section III. Accuracy studies of the method are carried out with the two-dimensional linear wave equation and Burgers' equation in Section IV. Each order of accuracy is numerically verified with five unstructured grids of consecutive refinement. Numerical solutions of plane electromagnetic waves incident on perfectly conducting circular cylinders and spheres are presented and compared with the exact solutions also in Section IV. Finally, some concluding remarks and suggestions for future study are given in Section V.

II. The Spectral Difference Method

A. General description

The partitioning of grid cells into subcells in the SV method is dictated by the need to satisfy the integral conservation law for each cell in order to capture discontinuities. It is then natural to define cell averages of conservative variables as discrete unknowns. But the flux integral for each grid cell can only be evaluated approximately. The accuracy of the flux at any point depends on the accuracy of the conservative variables, which is limited by the degree of precision of its reconstruction from the discrete unknowns. If the flux is non-linear, the surface integral is evaluated as a weighted sum of values at quadrature points, which is also accurate up to a certain degree of precision. Thus the unknowns can only be updated with an accuracy of a certain degree of precision. It is therefore sufficient to define the conservative unknowns at quadrature points that will approximate the volume integral over the cell to the desired order of accuracy, and that support a polynomial reconstruction of the desired degree of precision. Similarly, the flux will be defined at a different set of points, some or all of which lie on the cell boundary. They are located so that quadrature approximations for surface integrals over the cell boundaries exist to a required order of accuracy. The unknowns are updated using the differential form of the conservation law. Therefore the flux points must support a polynomial reconstruction of one higher degree of precision than the one for the conservative unknowns. Their location must also be chosen such that the integral conservation law for each grid cell is satisfied to the desired order of accuracy. If the nodes are distributed in a geometrically similar manner for all cells, the discretizations become universal, and can be expressed as the same weighted sums of the products of the local metrics and fluxes. These metrics are constants for the line, triangle, and tetrahedron elements, and can be computed analytically for curved elements. In this paper we only consider simplex cells with straight edges and planar faces. Further details are given in [13].

B. Details of the spectral difference method

The most general form of a conservation law can be written as

$$\frac{\partial u}{\partial t} + \nabla * F = 0, \tag{1}$$

where the conservative variable u can be a scalar or a vector, and the generalized flux F can be a vector or tensor. The term $\nabla * F$ represents the divergence or curl of F, depending on the physical definition of u. Integrating (1) over cell i, we obtain

$$\frac{d}{dt}\int_{V_i} u\,dV + \sum_{l=1}^{d+1}\int_{S_i^l} d\mathbf{S} * F = 0, \tag{2}$$

where V_i is the volume of the cell i, and $\mathbf{S}_i^l$ is the area vector of face l for cell i. (In 2D, each face is actually a line.) Here d is the dimension of the domain, and the number of faces for each cell is $d+1$.

In each cell, the discrete unknowns are the values of u at quadrature points for the volume integral over the cell. We denote these points, some of which may lie on the cell faces, as $\mathbf{r}_{j,i}$, and define $u_{j,i}$ as $u(\mathbf{r}_{j,i})$. The expansion of u in the cell can be written in the cardinal form

$$u_i(\mathbf{r}) = \sum_{j=1}^{N_p^d} L_{j,i}(\mathbf{r})\, u_{j,i}, \tag{3}$$

where $L_{j,i}(\mathbf{r})$ are the cardinal basis functions and N_p^d is the number of basis functions required to support a desired degree of precision p of the reconstruction, and is given by

$$N_p^d = \frac{(p+d)!}{p!d!}. \tag{4}$$

We will use polynomials as an independent basis. The locations of $\mathbf{r}_{j,i}$ then uniquely define the $L_{j,i}(\mathbf{r})$.

In order to evaluate the surface integrals in (2) efficiently, we discretize F at points $\mathbf{r}_{k,i}$, most or all of which are located at quadrature points for those integrals. If we define $F_{k,i}$ as $F(u(\mathbf{r}_{k,i}))$, the expansion of F in the cell can also be written in the cardinal form

$$F_i(\mathbf{r}) = \sum_{k=1}^{N_{p+1}^d} M_{k,i}(\mathbf{r})\, F_{k,i}, \tag{5}$$

where $M_{k,i}(r)$ are now the set of cardinal basis functions defined by $\mathbf{r}_{k,i}$. We can satisfy (1) at points $\mathbf{r}_{j,i}$ by evaluating

$$\nabla * F(\mathbf{r}_{j,i}) = \sum_{k=1}^{N_{p+1}^d} \nabla M_{k,i}(\mathbf{r}_{j,i}) * F_{k,i}. \tag{6}$$

In order to evaluate $F_{k,i}$, $u_{k,i}$ is required, which can be obtained directly from (3) as

$$u_{k,i} = \sum_{j=1}^{N_p^d} L_{j,i}(\mathbf{r}_{k,i})\, u_{j,i}. \tag{7}$$

To reduce the cost of this interpolation, some of points $\mathbf{r}_{k,i}$ may be chosen to coincide with $\mathbf{r}_{j,i}$. If the points $\mathbf{r}_{j,i}$ and $\mathbf{r}_{k,i}$ are distributed in a geometrically similar manner for all cells and within each cell i the gradient of a function is expressed in terms of its area vectors $\mathbf{S}_i^l$, the coefficients in (6) and (7) become universal, independent of cell i. Therefore, one can express these coefficients as

$$L_{j,i}(\mathbf{r}_{k,i}) = l_{kj}, \tag{8}$$

and

$$\nabla M_{k,i}(\mathbf{r}_{j,i}) = \frac{-1}{dV_i}\sum_{l=1}^{d} m_{jk,l}\,\mathbf{S}_i^l, \tag{9}$$

where we have chosen d of the area vectors $\mathbf{S}_i^l$ as basis vectors. There are only a few of these coefficients, which can be calculated exactly and stored in advance. Equations (7) and (6) can thus be rewritten as

$$u_{k,i} = \sum_{j=1}^{N_p^d} l_{kj}\, u_{j,i}, \tag{10}$$

and

$$\nabla * F(\mathbf{r}_{j,i}) = \frac{-1}{dV_i}\sum_{l=1}^{d} \mathbf{S}_i^l * \sum_{k=1}^{N_{p+1}^d} m_{jk,l} F_{k,i}. \tag{11}$$

For those points $\mathbf{r}_{k,i}$ located on the cell faces, since u may be discontinuous, we must replace the flux components $\mathbf{n} * F$ by a Riemann flux [10,12,14-15]. Here $\mathbf{n}$ is defined as the unit vector outward normal to the face. The other

flux components either remain unchanged in each cell or are simply set to the arithmetic averages of the values on the two sides of the face.

There are possible circumstances in which the reconstruction matrix for u or F is singular. In such a case, we can choose a different set of points. Alternatively, we can add additional points, generally one point at the centroid of the cell, to remove the singularity. We then use a least-squares method, the same one used in the FV method [1,6,10], for the reconstruction. All the equations above are still valid, except the upper limits must be suitably altered.

In order to check the integral conservation law for the cell, we evaluate the volume integral

$$\int_{V_i} \nabla * F \, dV = V_i \sum_{j=1}^{N_p^d} w_j \nabla * F(\mathbf{r}_{j,i}) = -\frac{1}{d} \sum_{l=1}^{d} \sum_{j=1}^{N_p^d} \sum_{k=1}^{N_{p+1}^d} w_j \, m_{jk,l} \, \mathbf{S}_i^l * F_{k,i} \,. \tag{12}$$

Here w_j are the volume quadrature weights at the points $\mathbf{r}_{j,i}$. We can also evaluate the surface integral of F as

$$\sum_{l=1}^{d+1} \int_{S_i^l} d\mathbf{S} * F = \sum_{l=1}^{d+1} \mathbf{S}_i^l * \sum_k w_k F_{k,i} \,. \tag{13}$$

Here w_k are surface quadrature weights for face l, and for each face the summation is over those points $\mathbf{r}_{k,i}$ located on that face. In order that the local integral conservation (2) is exactly satisfied numerically, Eq. (12) and the resulting equation of (13) using the relation $\sum_{l=1}^{d+1} \mathbf{S}_i^l = 0$ must have the same coefficient for each $F_{k,i}$. In particular, the total contribution from any interior point $F_{k,i}$ to the volume integral in (12) must vanish.

The SD formulation for the line element is a generalization of the multi-domain spectral method [8,9]. In [8,9], the u points were chosen at Gauss quadrature points and the F points at Gauss-Lobatto points. Here the distributions of u and F points are based on those quadrature points that lead to the satisfaction of the integral form of the conservation law. Since this does not define a unique set of locations, they can be optimized by minimizing some object functions. The tensor products of the line formulation can be used for quadrilateral and hexahedral cells or elements.

From Eqs. (10) and (11), we also see that the SD formulation is very similar to that of the FD method for structured grids. The SD method thus retains the simplicity and computational efficiency of the structured FD method. However, the metric terms in the latter are evaluated by numerically differencing the grid point coordinates. Since numerical grid generators are mostly only second-order accurate, the overall accuracy of the solution can be severely degraded if the grid is not sufficiently smooth. In contrast, the metric terms in the SD method are computed exactly from the geometry of the grid, no matter how it was generated. It thus retains its formal accuracy, even for very unsmooth unstructured grids. Furthermore, in contrast to the FD method, the integral conservation law is satisfied to the desired accuracy.

III. Locations of the Unknown and Flux Points

The critical part of the SD method is the location of the u points $\mathbf{r}_{j,i}$ and F points $\mathbf{r}_{k,i}$. If those points are distributed in a geometrically similar manner for all cells, the formulas for the flux derivatives become universal, and can be expressed as the same weighted sums of the products of the local metrics and fluxes. The locations of the u and F points are determined by symmetry groups associated with the cell centroids, vertices, edges, and faces [11]. All but the first contain arbitrary parameters that can be varied to obtain optimum solutions. The number of points required for a reconstruction with a specified degree of precision is greater than the minimum number of Gaussian quadrature points for that precision. One can obtain greater efficiency by locating some u points to coincide with F points. For F points on the vertices in 2D and edges and vertices in 3D, more than one Riemann solver is necessary. For those formulations with expensive Riemann solvers, these points should be minimized. Another criterion for the placement of u and F points is that the reconstruction matrix is nonsingular, if possible. If additional points are needed, the rank of the reconstruction matrix must be the same as the number of basis functions used. Even in this case, we can show that the number of F points is far less than the number of flux quadrature

points in the SV method with the same accuracy. The final criterion is that integral conservation is satisfied within the desired degree of precision.

Equation (4) gives the minimum number of points required in a reconstruction that support a polynomial of degree p. If the u points support a polynomial of degree p, the F points must support a polynomial of degree $p+1$, and the order of accuracy of the method is $p+1$. While the accuracy of the SD method depends on the locations of u and F points, here we present only some representative placements of u and F points that satisfy the integral conservation law, for various orders of accuracy. These placements do not necessarily represent the best choices, but they do show the orders of accuracy as claimed in our numerical tests. Due to space limitation, the exact locations of these points as well as the corresponding coefficients l_{kj} and $m_{jk,l}$ can be obtained by contacting the first author. Some data are also presented in [13].

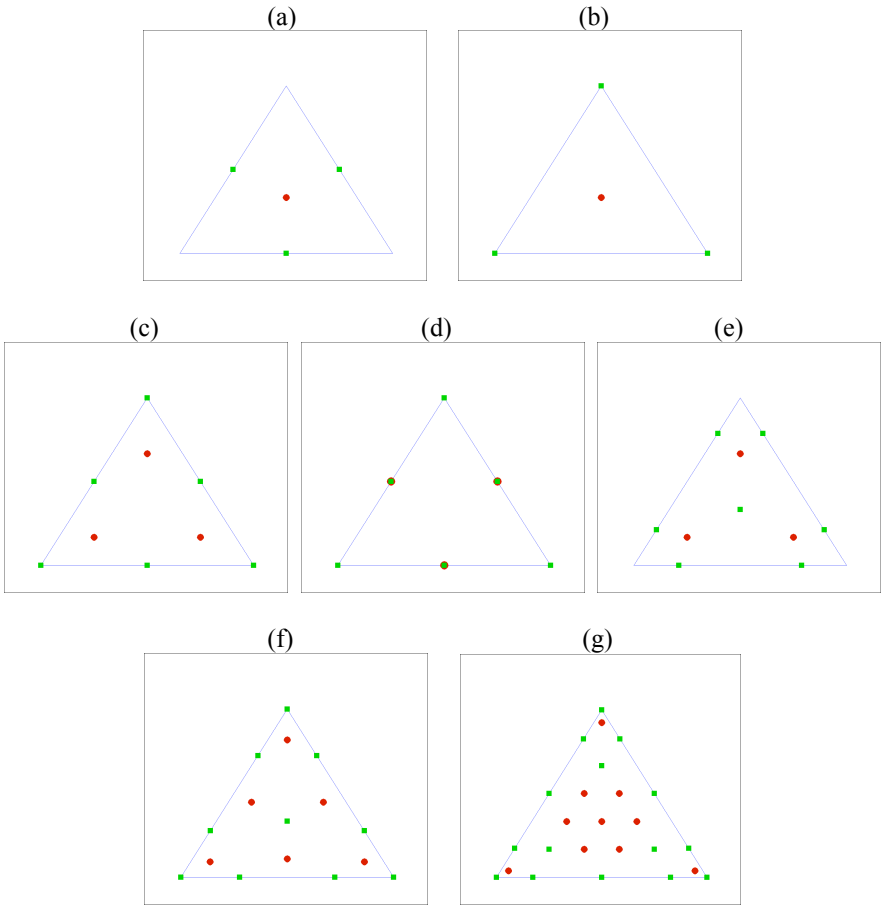

Figure 1. Placement of unknown and flux points for a triangular element.

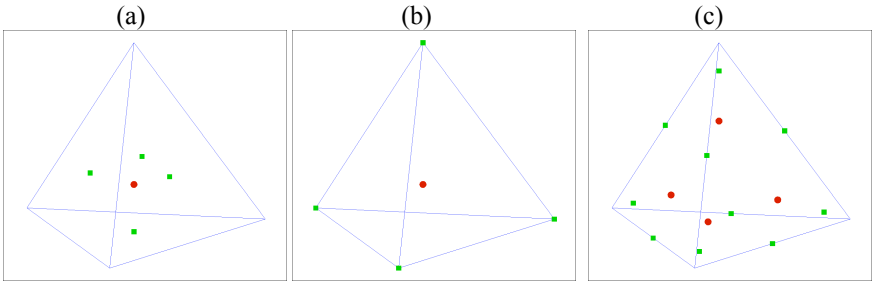

Figure 2. Placement of unknown and flux points for a tetrahedral element.

In Fig. 1 we show the placements of u points (circles) and F points (squares) for the triangle. Figures 1a and 1b show two different placements of the F points for first order accuracy. Three different second-order accurate placements are shown. In Fig. 2c, the u points are at the Gaussian quadrature points, while the F points are at the Gauss-Lobatto points on the edges. In Fig. 2d the u points are moved to the other Gauss points on the midedges, where they coincide with F points. Moving the F points to the Gaussian points on the edges in order to minimize Riemann solver calls results in a singular matrix. The singularity is removed by adding an additional F point at the centroid as shown in Fig. 2e. Figures 1f and 1g show a third-order accurate and a fourth-order accurate placement, respectively. While the former has one interior F point and the latter has three, the

boundary F points are at their Gauss-Lobatto points on the edges and the u points are at a fifth-order accurate volume quadrature points for both cases. In Fig. 2 we show several placements of the points for the tetrahedral element. Figures. 2a and 2b show two different placements of the F points for first order accuracy, while the u point is at the centroid. A second-order accurate placement of points is shown in Fig. 3c. The u points are located at the Gaussian quadrature points. Six of the F points are on the edge midpoints, while the remaining four vertex-based points are at some arbitrary interior points. In all placements presented here, the local integral conservation is exactly satisfied numerically. In addition, the geometrical conservation is also satisfied.

IV. Numerical Results

A. Accuracy study with 2D linear wave equation

We first test the accuracy of the SD method on the two-dimensional linear wave equation

$$\frac{\partial u}{\partial t}+\frac{\partial u}{\partial x}+\frac{\partial u}{\partial y}=0, \qquad -1\le x\le 1, \quad -1\le y\le 1, \tag{14}$$
$$u(x,y,0)=\sin\pi(x+y), \qquad \textit{periodic boundary condition}.$$

A 10x10x2 unstructured grid over the square domain $(-1\le x\le 1,-1\le y\le 1)$ is shown in Fig. 3. Note that the cells in the irregular grid have quite different sizes. Five grids of consecutive refinement were used in the study. The finer grids were generated recursively by cutting each coarser grid cell into four finer grid cells. The boundary fluxes on each triangular element's face were computed fully upwinded. The initial condition is $u_0(x,y)=\sin\pi(x+y)$. This solution is then updated at each time step using a third-order TVD Runge-Kutta scheme [16]. The numerical simulation was carried until t = 1. In Fig.4a, we plot the L_1 and L_∞ error norms using the first to fourth order SD schemes with the u and F placements given in Figs. 1a, 1c, 1f, and 1g, respectively. The errors presented in the figure are time independent because the time step Δt was made small enough so that the errors are dominated by the spatial discretization. It is easily verified from the figure that all schemes are convergent with grid refinement and the expected orders of accuracy have been achieved. In Fig. 4b, we show the same error norms using the second to fourth order SV schemes [19]. It is shown that the SD method has similar errors as the SV method in this test.

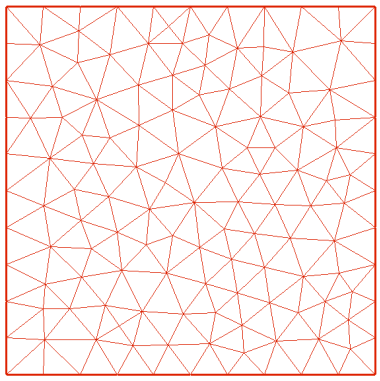

Figure 3. An unstructured grid over a square domain.

(a) SD (b) SV

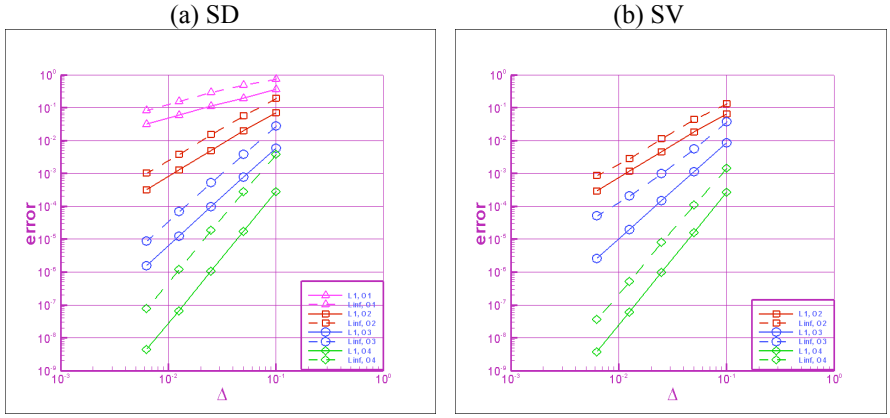

Figure 4. Error Norms of various order of accuracy for the 2D linear wave equation at t=1.0.

B. Burgers' equation and shock capturing

In this case, we test the accuracy of the SD method on the two-dimensional Burgers' equation:

$$\frac{\partial u}{\partial t}+\frac{\partial u^2/2}{\partial x}+\frac{\partial u^2/2}{\partial y}=0, \qquad -1\le x\le 1, \quad -1\le y\le 1,$$
$$u(x,y,0)=\frac{1}{4}+\frac{1}{2}\sin\pi(x+y), \qquad \textit{periodic boundary condition}. \tag{15}$$

The test was carried out using the same first to fourth order SD schemes and the same time integration scheme on the same grids as used in the previous test. The boundary fluxes on each element's face were first computed fully upwinded. We started with a smooth initial solution. Due to the non-linearity of the Burgers equation, discontinuities will develop in the solution. At t = 0.1, the exact solution is still smooth. The numerical simulation was therefore carried out until t = 0.1 without the use of limiters. In Fig. 5a, we present the L_1 and L_∞ errors of the four SD schemes. The performance of the SD method on the non-linear Burgers equation is very good. All schemes are convergent with grid refinement and the expected orders of accuracy have been achieved, although there is a slight loss of accuracy in the L_∞ norm, probably due to the non-linear nature of the Burgers equation. In Fig. 5b, we also show the same error norms using the second to fourth order SV schemes [19]. Again, the SD method has similar errors as the SV method in this test. We then carried out the test with a different way to compute the boundary fluxes. On each

(a) SD (b) SV

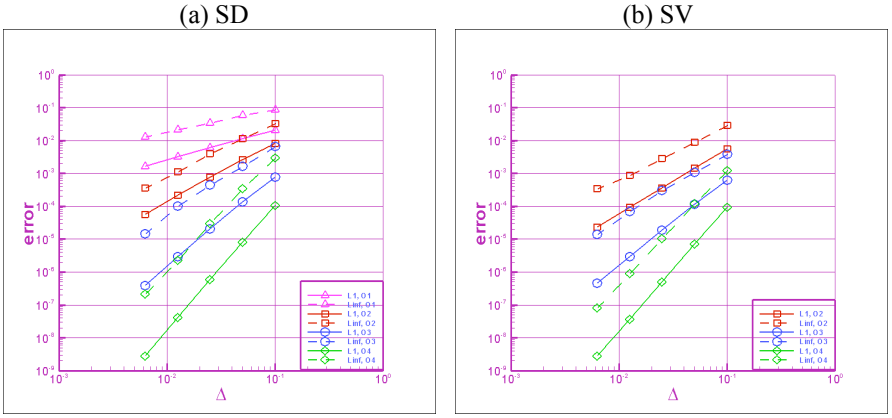

Figure 5. Error Norms of various order of accuracy for the 2D Burgers' equation at t=0.1.

(a) exact (b) second-order SD

(c) third-order SD (d) fourth-order SD

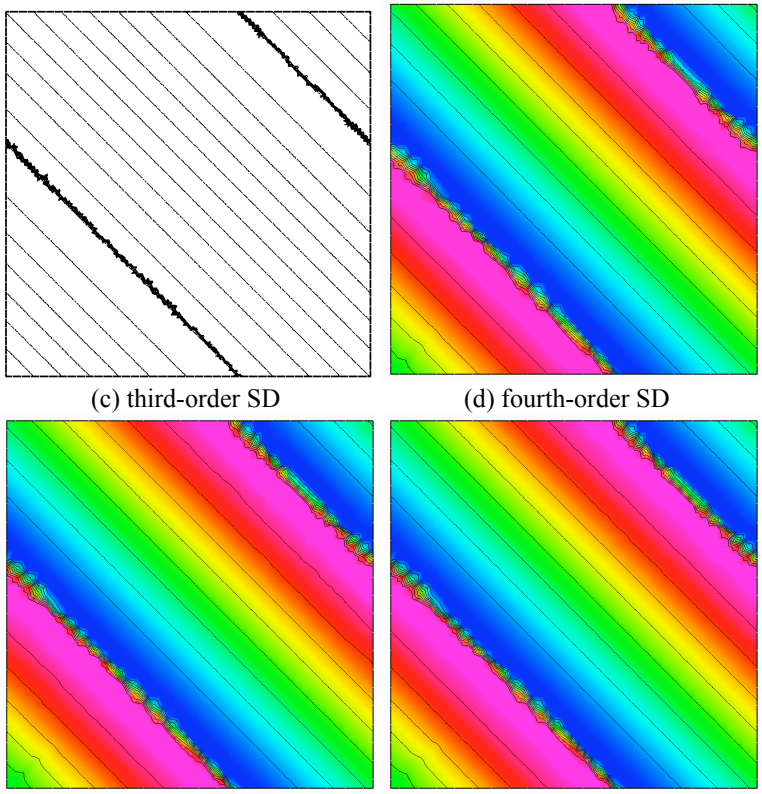

Figure 6. Solutions of 2D Burgers' equation at t = 0.45

face, the normal component of the flux at every flux point was first computed with the Rusanov Riemann flux [15]. The full flux was then determined with the two Riemann fluxes at each vertex of every element, while it was determined with the Riemann flux and the original tangential flux at other flux points on the face. The errors are similar to the previous test with fully upwind fluxes. At t = 0.45, the exact solution has developed two shock waves, and limiters were then used to handle the discontinuities. A TVD limiter implemented here is very similar to that for the SV method [19]. Shown in Figure 6 are the exact solution and the numerical solutions with the second, third, and fourth order SD schemes using fully upwind boundary fluxes on the 40x40x2 irregular grid. The shock waves are captured well in all cases.

C. Scattering of an electromagnetic plane wave incident on a perfectly conducting cylinder and sphere

In order to demonstrate the high accuracy of the method, it was decided in this initial phase to choose problems for which there exist exact solutions. To this end we solve the Maxwell equations

$$\frac{\partial \mathbf{D}}{\partial t} - \nabla \times \mathbf{H} = 0 \tag{16a}$$

$$\frac{\partial \mathbf{B}}{\partial t} + \nabla \times \mathbf{E} = 0. \tag{16b}$$

The electric and magnetic flux density vectors $(\mathbf{D}, \mathbf{B})$ and the intensity vectors $(\mathbf{E}, \mathbf{H})$ are related through the constitutive relations

$$\mathbf{D} = \varepsilon \mathbf{E} \tag{17a}$$

$$\mathbf{B} = \mu \mathbf{H}, \tag{17b}$$

where ε is the permittivity and μ is the permeability of the material. Exact solutions exist for plane waves incident on simple bodies in two and three dimensions. The time integration scheme and the Riemann solver used here are the same ones previously used in the SV paper [12].

For the first test case, we considered a plane wave incident on a perfectly conducting circular cylinder. Calculations were carried out over an unstructured grid consisting of 2024 cells, shown in Fig. 7a. The cylinder is approximated with a 32-sided polygon. The outer boundary is two radii away from the body surface, with no PML (perfectly matched layer). This gives approximately $30/ka$ cells per wavelength, or approximately $30\sqrt{n(n+1)}/ka$ unknowns per wavelength. Here k is the wave number, a is the radius of the cylinder, and $n = p+1$ is the order of the accuracy of the method. The incident wave with $ka = 5$ is propagating from left to right. Figures 7b to 7f show contour plots of E_z for a TM wave as calculated using the first to fourth order SD schemes with the u and F placements given in Figs. 1a, 1c, 1e, 1f, and 1g. We have also plotted the exact solution (solid lines) on the same figures for easy comparisons. It is seen that the first order solution is very dissipative with this resolution. While both second-order solutions captured all the main features of the wave, the scheme using the least-squares formulation is more accurate. The third and fourth order solutions show an excellent agreement with the exact solution. Similar results were obtained for a TM wave also. Figures 8a to 8c show the contour plots for a wave with $ka = 10$ using the second to fourth order SD schemes. With the grid resolution reduced by a factor of two, the second-order scheme now is unable to produce an accurate solution. The third-order scheme can still capture the main features of the wave, but is a little bit too dissipative. Nevertheless, the fourth-order scheme agrees very well with the exact solution. We next tested the SD schemes on a grid in which the outer boundary is much closer to the body. Figure 9a shows a grid consisting of 226 cells with the same resolution, but the outer boundary is only a half radius away from the body. Numerical solutions of the third and fourth order SD schemes are plotted in Fig. 9b and 9c, respectively. They agree well with the exact solution, attesting to the accuracy of the numerical non-reflecting boundary procedure.

For three-dimensional cases, the Maxwell equations pose a challenge for the SD method. This is because each Riemann solver gives two tangential components of each $\mathbf{E}$ and $\mathbf{H}$ field, and therefore fluxes at any point on the vertices or edges of the tetrahedral cell are over-determined. Further research is required to solve this problem. Here we only considered a plane wave incident on a perfectly conducting sphere using the first-order SD scheme with the u and F placements given in Fig. 2a. Figure 10a shows the unstructured grid, consisting of 113352 tetrahedral cells. The outer boundary is two radii away from the body surface, also with no PML. This gives approximately $30/ka$ cells or $30\sqrt[3]{n(n+1)(n+2)}/ka$ unknowns per wavelength for the first-order scheme. The incident wave,

propagating in the positive z direction, has an x component for the **E** field and a y component for the **H** field, with $ka = 1$. Figures 10b shows the color contours of E_x plotted on the sphere, plane of symmetry, and the outer boundaries. The exact solution is also plotted on the same figures with solid contour lines for easy comparisons. With 55 unknowns per wavelength, the first-order solution actually agreed very well with the exact solution, even at the outer boundaries. Fig. 10c shows the result for $ka = 3$, indicating that the first-order scheme is now very dissipative.

V. Concluding Remarks

In this paper, we presented a new, high-order, conservative, and efficient method for conservation laws on unstructured grids. The method combines the best features of structured and unstructured grid methods in which the structured distribution of discrete variables in each unstructured cell maintains computational efficiency and geometric flexibility. It utilizes the concept of discontinuous and high-order local representations to achieve conservation and high accuracy. Universal reconstructions are obtained by distributing unknown and flux points in a geometrically similar manner for all unstructured cells. The flux derivatives needed to update the conservative unknowns are expressed as universal weighted sums of the fluxes, leading to great computational efficiency. An important aspect of the method is that the number of Riemann solvers per unknown decreases as the order of accuracy increases, reducing the cost for higher order. Placements of the unknown and flux points with various orders of accuracy are given for triangular and tetrahedral elements. Accuracy studies of the method are carried out with the two-dimensional linear wave equation and Burgers' equation, and each order of accuracy is numerically verified. Numerical solutions of plane electromagnetic waves incident on perfectly conducting circular cylinders and spheres are presented and compared with the exact solutions to demonstrate the capability of the method. Excellent agreements have been found. Further improvements include extension to high orders in three dimensions, curved boundaries, optimization of unknown and flux placements, implicit time integration, grid and order adaptation, multidimensional limiters and filters, and moving grids.

References

[1]J. Barth and P.O. Frederickson, High-order solution of the Euler equations on unstructured grids using quadratic reconstruction, AIAA Paper No. 90-0013 (1990).

[2]B. Cockburn and C.-W. Shu, TVB Runge-Kutta local projection discontinuous Galerkin finite element method for conservation laws II: general framework, *Mathematics of Computation* **52**, 411-435 (1989).

[3]B. Cockburn, S.-Y. Lin and C.-W. Shu, TVB Runge-Kutta local projection discontinuous Galerkin finite element method for conservation laws III: one-dimensional systems, *J. Comput. Phys.* **84**, 90-113 (1989).

[4]B. Cockburn, S. Hou and C.-W. Shu, TVB Runge-Kutta local projection discontinuous Galerkin finite element method for conservation laws IV: the multidimensional case, *Mathematics of Computation* **54**, 545-581 (1990).

[5]B. Cockburn and C.-W. Shu, The Runge-Kutta discontinuous Garlerkin method for conservation laws V: multidimensional systems, *J. Comput. Phys.*, **141**, 199 - 224, (1998**).**

[6]M. Delanaye and Y. Liu, Quadratic reconstruction finite volume schemes on 3D arbitrary unstructured polyhedral grids, AIAA Paper No. 99-3259-CP, 1999.

[7]T.J.R. Hughes, The finite element method, linear static and dynamic finite element analysis, Prentice-Hall, Inc., 1987.

[8]D.A. Kopriva and J.H. Kolias, A conservative staggered-grid Chebyshev multidomain method for compressible flows, *J. Comput. Phys.* **125**, 244 (1996).

[9]D.A. Kopriva and J.H. Kolias, A conservative staggered-grid Chebyshev multidomain method for compressible flows. II semi-structured method, *J. Comput. Phys.* **128**, 475 (1996).

[10]Y. Liu, A generalized finite volume algorithm for solving Maxwell's equations on arbitrary grids, Proceedings of 10th Annual Review of Progress in Applied Computational Electromagnetics, 1994.

[11]Y. Liu and M. Vinokur, Exact integration of polynomials and symmetric quadrature formulas over arbitrary polyhedral grids, *J. Comput. Phys.* **140**, 122-147 (1998).

[12]Y. Liu, M. Vinokur, and Z.J. Wang, Spectral (finite) volume method for conservation laws on unstructured grids V: extension to three-dimensional systems, submitted to *J. Comput. Phys.* 2004.

[13]Y. Liu, M. Vinokur, and Z.J. Wang, Spectral difference method for unstructured grids I: basic formulation, to be submitted to *J. Comput. Phys.* 2005.

[14]P.L. Roe, Approximate Riemann solvers, parameter vectors, and difference schemes, *J. Comput. Phys.* **43** 357-372 (1981).

[15]V.V. Rusanov, Calculation of interaction of non-steady shock waves with obstacles, *J. Comput. Math. Phys. USSR* **1**, 267-279 (1961).
[16]C.-W. Shu, Total-variation-diminishing time discretizations, *SIAM J. Sci. Stat. Comput*. **9**, 1073 (1988).
[17]D. Sridar and N. Balakrishnan, An upwind finite difference scheme for meshless solvers, *J. Comput. Phys.* **189** 1-29 (2003).
[18]Z.J. Wang, Spectral (finite) volume method for conservation laws on unstructured grids: basic formulation, *J. Comput.*

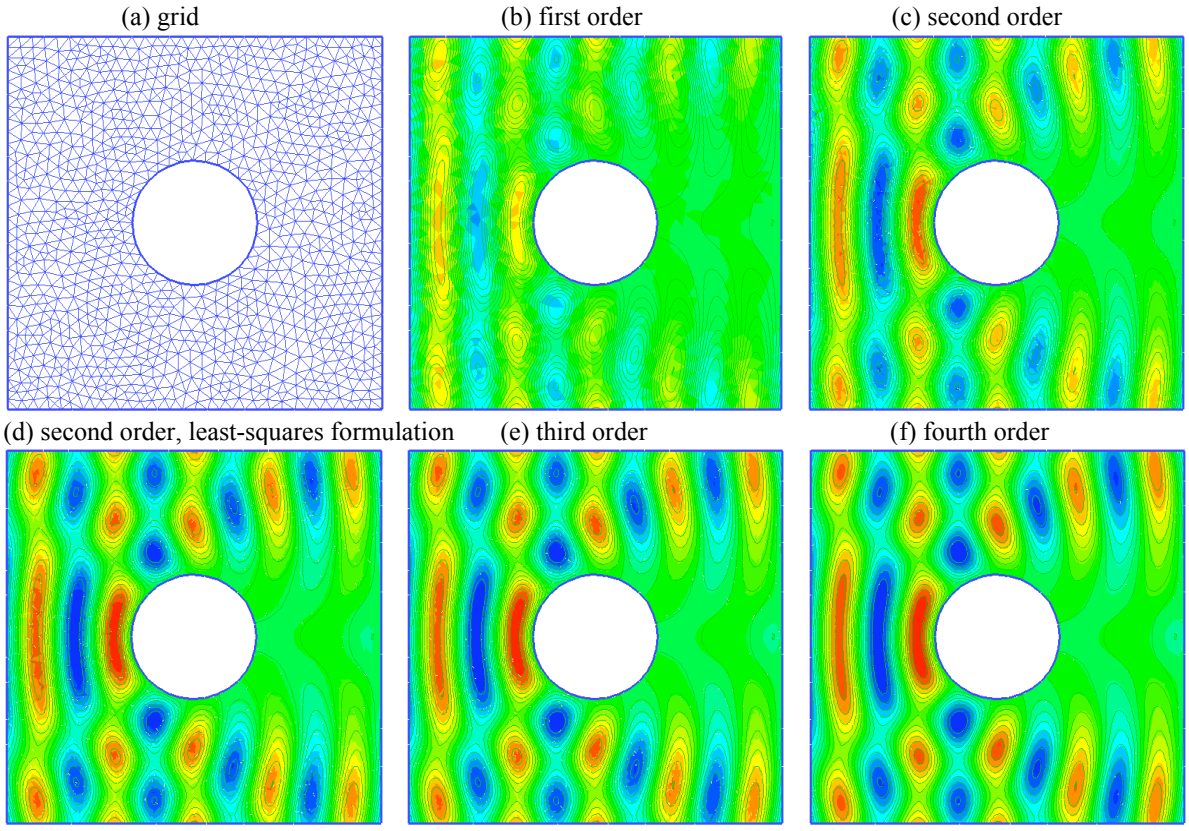

Figure 7. Contour plot of E_z for a plane wave (ka = 5) incident on a perfectly conducting cylinder.

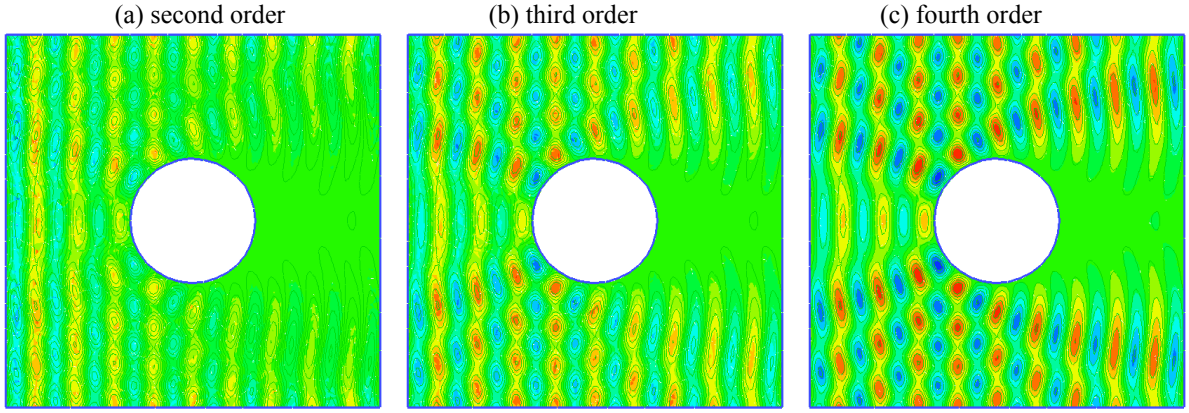

Figure 8. Contour plot of E_z for a plane wave (ka = 10) incident on a perfectly conducting cylinder.

Phys. **178**, 210 (2002).
[19]Z.J. Wang and Y. Liu, Spectral (finite) volume method for conservation laws on unstructured grids II: extension to two-dimensional scalar equation, *J. Comput. Phys*. **179**, 665-697 (2002).
[20]Z.J. Wang and Y. Liu, Spectral (finite) volume method for conservation laws on unstructured grids III: one-dimensional systems and partition optimization, *J. Scientific Comput*. **20**, 137-157 (2004).
[21]Z.J. Wang, L. Zhang, and Y. Liu and, Spectral (finite) volume method for conservation laws on unstructured grids IV: extension to two-dimensional systems, *J. Comput. Phys*. **194**, 716-741 (2004).

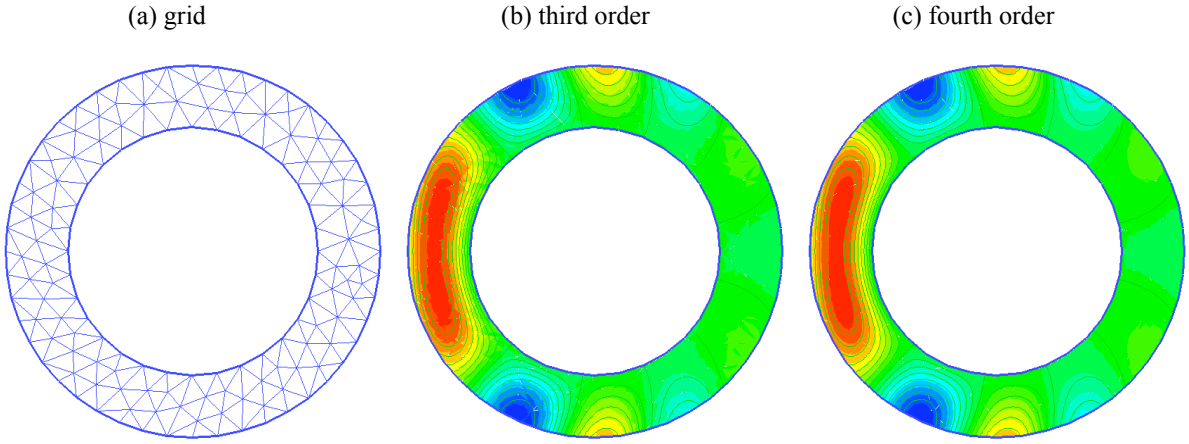

Figure 9. Contour plot of E_z for a plane wave (ka = 5) incident on a perfectly conducting cylinder.

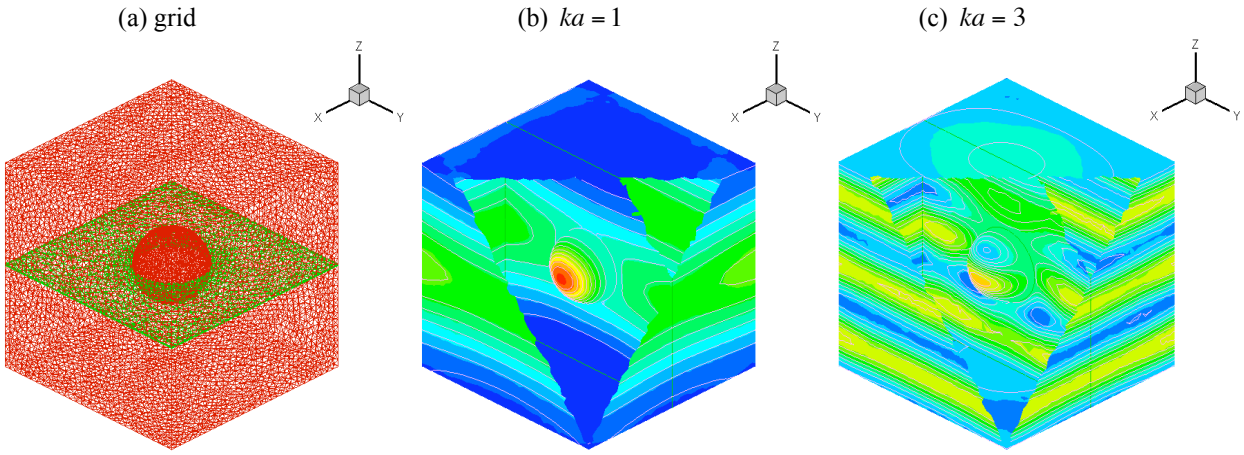

Figure 10. Contour plot of E_x for a plane wave incident on a perfectly conducting sphere.